

Ion Pairing and Redissociation in Low-Permittivity Electrolytes for Multivalent Battery Applications

Julian Self, Nathan T. Hahn, Kara D. Fong, Scott A. McClary, Kevin R. Zavadil, and Kristin A. Persson*

Cite This: *J. Phys. Chem. Lett.* 2020, 11, 2046–2052

Read Online

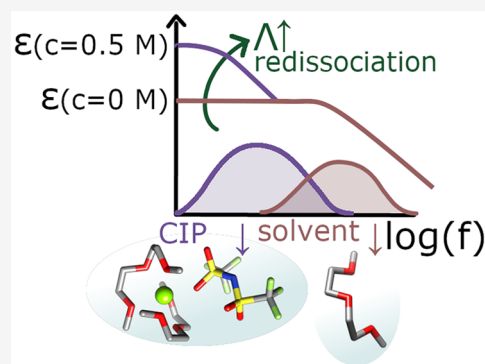
ACCESS |

Metrics & More

Article Recommendations

Supporting Information

ABSTRACT: Detailed speciation of electrolytes as a function of chemical system and concentration provides the foundation for understanding bulk transport as well as possible decomposition mechanisms. In particular, multivalent electrolytes have shown a strong coupling between anodic stability and solvation structure. Furthermore, solvents that are found to exhibit reasonable stability against alkaline-earth metals generally exhibit low permittivity, which typically increases the complexity of the electrolyte species. To improve our understanding of ionic population and associated transport in these important classes of electrolytes, the speciation of $\text{Mg}(\text{TFSI})_2$ in monoglyme and diglyme systems is studied via a multiscale thermodynamic model using first-principles calculations for ion association and molecular dynamics simulations for dielectric properties. The results are then compared to Raman and dielectric relaxation spectroscopies, which independently confirm the modeling insights. We find that the significant presence of free ions in the low-permittivity glymes in the concentration range from 0.02 to 0.6 M is well-explained by the low-permittivity redissociation hypothesis. Here, salt speciation is largely dictated by long-range electrostatics, which includes permittivity increases due to polar contact ion pairs. The present results suggest that other low-permittivity multivalent electrolytes may also reach high conductivities as a result of redissociation.



One of the impediments toward improving Mg electrochemistry is the lack of a fundamental understanding of the governing electrochemical and physiochemical properties of the electrolyte. Although there exists a significant body of work focusing on transport properties, solvation, and electrochemical stability,^{1–6} ion pairing and speciation remain poorly understood for commonly studied multivalent electrolyte systems,⁷ despite their crucial importance to overall electrolyte behavior. A critical leap in understanding of multivalent electrolytes is needed to accelerate their development and achieve parity with lithium electrolytes.

Most Li ion and specifically high-permittivity electrolytes studied for electrochemical applications exhibit a decreasing molar conductivity with increasing concentration,⁸ as ion pairing and viscosity increase. In contrast, multivalent electrolytes (which are generally prepared with solvents of low static permittivity,² e.g., $\epsilon < 10$) can show an increasing molar conductivity Λ (concentration-normalized conductivity) with increasing concentration. More precisely, in concentration ranges of electrochemical interest (e.g., 0.01 to 1 M), the molar conductivity initially increases and eventually reaches a maximum at moderate concentrations. The initial increase in molar conductivity for low-permittivity multivalent electrolytes may be due to a dramatic, more complex change in ion speciation compared with high-permittivity monovalent electrolytes.

Two representative low-permittivity multivalent Mg^{2+} electrolytes are magnesium bis(trifluoromethylsulfonyl)imide, $\text{Mg}(\text{TFSI})_2$, in monoglyme (G1) and $\text{Mg}(\text{TFSI})_2$ in diglyme (G2), which have been widely investigated for use in electrochemical cells,² primarily because of their high conductivity, solubility, and commercial availability. These anion–solvent combinations are also widely utilized for lithium–oxygen and lithium–sulfur electrochemistry.^{9–11} However, $\text{Mg}(\text{TFSI})_2$ in ethers requires an additional salt (e.g., MgCl_2) in order to allow plating and stripping at high Coulombic efficiencies.² Nonetheless, the present work will focus specifically on $\text{Mg}(\text{TFSI})_2$ in ethers without an additional salt, as even such simple electrolytes, which are the subject of intense research and interest,^{3,4,6,12,13} are still poorly understood in terms of salt speciation¹⁴ and bulk thermodynamic properties.¹⁵

For $\text{Mg}(\text{TFSI})_2$ in both G1 and G2, the concentration-dependent molar conductivity deviates from that of high-permittivity electrolytes (Figure 1).^{15,16} The molar conductivity

Received: January 31, 2020

Accepted: February 20, 2020

Published: February 20, 2020

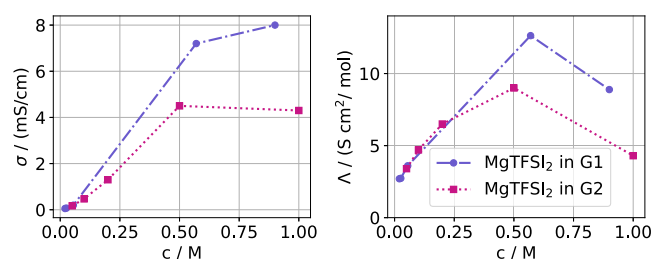


Figure 1. Measured conductivity (left) and molar conductivity (right) as functions of the concentration of $\text{Mg}(\text{TFSI})_2$ in G1 or G2 solvent.

ity increases with concentration, indicating nonconventional behavior: typically (e.g., for high-permittivity solvents) the molar conductivity decreases with increasing concentration in the dilute limit following Kohlrausch's law,¹⁷ and at concentrations of ~ 0.5 M following, among other factors, significant viscosity and ion pairing increases.¹⁸ The molar conductivity increase for G1 and G2 suggests that ion pairing decreases¹³ (i.e., the population fraction of charge carriers is increased), contrary to what would be expected from simple predictions based on the law of mass action.

Salama et al. suggested on the basis of diffusion and Raman measurements that $\text{Mg}(\text{TFSI})_2$ in G1 exists primarily as free ions independent of concentration,¹⁵ a finding that is under contention.^{6,7} Similarly, Kubisiak and Eilmes¹² reported molecular dynamics (MD) simulations that showed strictly solvent-solvated Mg^{2+} from 0.1 to 1 M $\text{Mg}(\text{TFSI})_2$ in G1. Sa et al. studied $\text{Mg}(\text{TFSI})_2$ in G2 and found an (unusual) increase in the diffusivity of the salt by an order of magnitude as the concentration increased from 0.1 to 0.7 M, which was suggested to be a result from a "complicated solution environment at different ionic strengths".¹⁶ Using MD they found a significant presence of solvent-separated ion pairs (SSIPs) or free ions and a monotonic increase in ion pairing with increasing concentration from 0.2 to 2 M. Unfortunately, the results from Salama et al., Kubisiak and Eilmes, and Sa et al. are not consistent with the relevant molar conductivity increase. Via X-ray and MD studies of 0.4 M $\text{Mg}(\text{TFSI})_2$ in G2, Lapidus et al.⁶ found that approximately half of the Mg^{2+} was free, with the remaining split into contact ion pairs (CIPs) or neutral triple ions. Kimura et al., who studied $\text{Mg}(\text{TFSI})_2$ in triglyme via conductivity and Raman measurements, suggested a shifting equilibrium between SSIPs and free ions as the concentration is varied to explain the increasing molar conductivity, but they did not provide a physical motivation for such a mechanism.¹³ The differences in the aforementioned interpretations and suggestions illustrate that no clear consensus has yet emerged regarding the speciation in low-permittivity multivalent systems.

We hypothesize that the interplay between ion pairing and molar conductivity can be rationalized via a phenomenon termed *redissociation*.^{19–23} In low-permittivity electrolytes, associated salt species tend to form as a result of the strong electrostatic interactions compared with polar solvents.²⁴ If these associated species are endowed with a significant dipole moment, they will increase the total permittivity via an increase in the orientational polarizability and favor a larger population of dissociated salt species, i.e., redissociation, as the concentration increases.^{21,22,25} Previous studies of the interplay between permittivity increase and ion association have focused on monovalent salts.^{19,21–23,25–27} To the best of our knowledge, redissociation has not been analyzed or proposed

for nonaqueous multivalent systems, despite the inherently stronger electrostatic interactions present.

Characterization of ion pairing for multivalent liquid electrolyte systems is quite challenging because of the strong interionic interactions in solution: many conventional techniques such as conductometry are often not directly applicable,²⁴ and the challenges are compounded for low-permittivity systems. In order to evaluate the redissociation hypothesis for low-permittivity multivalent electrolytes, herein we use a multiscale computational model (MSM) to predict the permittivity and salt speciation as functions of concentration. To verify the results, we use Raman spectroscopy and dielectric relaxation spectroscopy (DRS). While previous work on combined permittivity and speciation diagrams have used a posteriori experimental data,^{23,28,29} the current MSM is entirely theoretically and computationally based and relies on experimental data only for validation. Furthermore, a significant number of dielectric relaxation studies have been carried out on low-permittivity monovalent systems^{19,21,26,27} as well as some high-permittivity multivalent systems,²⁸ but to date none have been carried out on low-permittivity multivalent electrolytes, the subject of the present work.

For a system with divalent cations and monovalent anions, the concentration association constant K_A directly provides the ratio of the concentration of associated monocationic CIPs ($c_{\text{cip},+}$) to those of the free ions (c_{++} and c_-) via the following relationships:²⁴

$$K_A(c) = \frac{c_{\text{cip},+}}{c_{++}c_-} = K_A^0 \frac{\gamma_{++}\gamma_-}{\gamma_{\text{cip},+}} f_{e,A} \quad (1)$$

in which the thermodynamic association constant K_A^0 has been introduced as well as the concentration activity coefficients of the multivalent cation, anion, and contact ion pair (γ_{++} , γ_- , and $\gamma_{\text{cip},+}$ respectively), and the permittivity correction term $f_{e,A}$. K_A^0 accounts for specific short-range interactions, while the activity coefficients γ_i and the permittivity correction term $f_{e,A}$ account for long-range nonspecific electrostatic interactions.

With the assumption that only free ions and contact ion pairs are present, the following concentration conservation equation can be written:

$$c = c_{++} + c_{\text{cip},+} \quad (2)$$

Moreover, charge neutrality imposes the following condition:

$$2c_{++} + c_{\text{cip},+} = c_- \quad (3)$$

In the present work, K_A^0 is obtained through first-principles electronic structure calculations within a continuum solvation model enhanced with an explicit first solvation shell for the multivalent cation (see [Methods](#)). For low to moderate concentrations (e.g., up to 0.7 M), a Guggenheim-type equation is often used for activity coefficients,²⁸ where the first term is the Debye–Huckel expression; such a model is employed in the present work, as follows:^{28,30}

$$\frac{\gamma_{++}\gamma_-}{\gamma_{\text{cip},+}} = 10^{-4A_{\text{DH}}\sqrt{I}/(1+B_{\text{DH}}\alpha_{\text{DH}}\sqrt{I})} \quad (4)$$

In the above equation, the symbols have their typical significance:^{28,30} B_{DH} is the Debye–Huckel term, α_{DH} is the distance of closest approach, A_{DH} is the Debye–Huckel parameter, and I is the ionic strength. While Guggenheim-type expressions also include linear and higher-order terms in the ionic strength for the ions' chemical potential, here we assume

that the impact of terms in addition to the standard Debye–Hückel expression due to changes in permittivity is first-order.^{31,32} Thus, the role of such terms is fulfilled by $f_{\epsilon,A}$ described above. Hence, we neglect any higher-order corrections.

If the permittivity of the electrolyte remains fairly constant as a function of concentration, then $f_{\epsilon,A}$ would equal unity. However, if the permittivity changes appreciably, as it tends to do for low-permittivity electrolytes, then the following phenomenological equation can be used:¹⁹

$$f_{\epsilon,A} = \exp\left[-\frac{b}{\epsilon(c=0)} + \frac{b}{\epsilon(c)}\right] \quad (5)$$

where $\epsilon(c)$ is the concentration-dependent permittivity, $\epsilon(c=0)$ is the permittivity of the neat solvent, and b is a positive phenomenological constant.

With increasing concentration of charged species, the charged species' activity coefficients γ_i decrease and hence compete with the mass action law, which promotes association. If the permittivity increases, then this will act as an additional driving force for reduced association (and increased association if the permittivity decreases).

Together, eqs 1–5 allow for the construction of speciation diagrams from first-principles calculations provided that $\epsilon(c)$ is known in the desired concentration range. The concentration dependence of ϵ can be expressed as follows:

$$\epsilon(c) = \epsilon(c=0) + \sum_i \Delta\epsilon_i c_i + O(c_i^2) \quad (6)$$

where $\Delta\epsilon_i$ is the dielectric constant increment for species i . Here it is assumed that $\Delta\epsilon_i$ is independent of concentration and that higher-order terms can be neglected. When eq 6 is coupled to eqs 1–5, then the total permittivity can be calculated as a function of concentration provided that each $\Delta\epsilon_i$ is known. As described in Methods and in a previous publication,³³ $\Delta\epsilon_i$ can be calculated from classical MD simulations.

Figure 2 shows the static permittivity (dielectric constant) (top) and the speciation (bottom) as functions of concen-

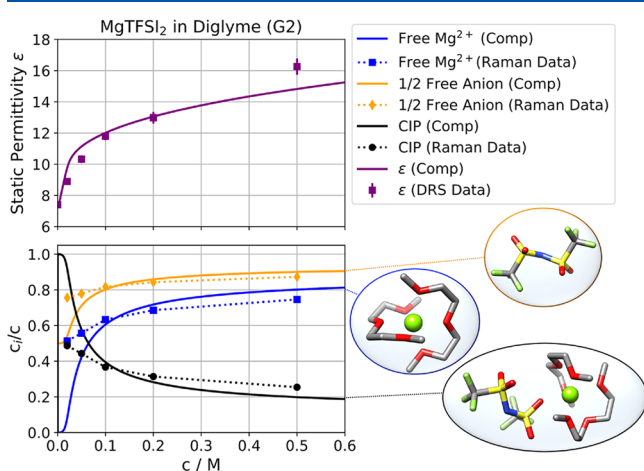


Figure 2. (top) Permittivity and (bottom) speciation diagram of $\text{Mg}(\text{TFSI})_2$ in G2 at 25 °C. In the speciation diagram, the solid lines show the computed species fractions c_i/c , except in the case of the anion, for which $0.5c_i/c$ is shown. Species in question are illustrated in bubbles.

tration for $\text{Mg}(\text{TFSI})_2$ in G2. The static permittivity is computed to increase from 7.4 (neat G2) to 14.8 (0.5 M), while it is measured to increase from 7.4 to 16.2. There is good agreement throughout the studied concentration range (0.02 to 0.5 M). The error bars are a consequence of the fitting procedure required to extract the static permittivity values from the frequency-dependent spectra (see Methods). The tendency of the permittivity to increase with concentration is different than what is observed for salts in typical high-permittivity electrolytes (e.g., NaCl in water), where the dielectric constant typically decreases with concentration as a result of the loss of free solvent molecules due to binding to the solvation shell of free ions, thus reducing the orientational polarizability of the solution.³⁴ Here, the increase in permittivity with concentration unequivocally indicates that associated species, e.g., CIPs, which have a strong dipole moment, are present in appreciable quantities in the solution.

The speciation inferred from the Raman analysis of TFSI ion pairing is in good agreement with the computed values (Figure 2, bottom). Here the population fractions of free ions increase with concentration while that of the associated species (i.e., CIPs) decreases, consistent with the molar conductivity increase.

Table 1 shows the computed dielectric increments for the salt species, which were used in the MSM. We note that

Table 1. Computed Dielectric Increments Per Mole of Species and K_A^0 Values

solvent	$\Delta\epsilon_{++}/\text{M}^{-1}$	$\Delta\epsilon_{-}/\text{M}^{-1}$	$\Delta\epsilon_{\text{CIP},+}/\text{M}^{-1}$	K_A^0
G2	-11	-3.0	147	5.2×10^8
G1	-13	-2.7	72	3.6×10^8

although the presence of free ions tends to lower ϵ , the decrease is much less than the increase in ϵ due to CIPs.

Figure 3 shows the static permittivity (top) and the speciation (bottom) as functions of concentration for $\text{Mg}(\text{TFSI})_2$ in G1. The static permittivity is computed to increase with concentration from 7.0 (neat G1) to 10.8 (0.57 M salt in

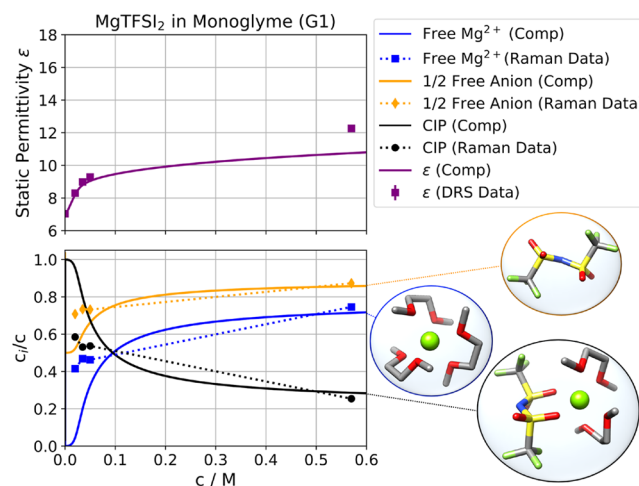


Figure 3. (top) Permittivity and (bottom) speciation diagram of $\text{Mg}(\text{TFSI})_2$ in G1 at 25 °C. In the speciation diagram, the solid lines show the computed species fractions c_i/c , except in the case of the anion, for which $0.5c_i/c$ is shown. Species in question are illustrated in bubbles.

G1) and is measured to increase from 7.0 to 12.3 by DRS, in general agreement. No data points were obtained between 0.05 and 0.57 M because of the miscibility gap in the electrolyte¹⁵ (see [Methods](#)).

The bottom panel of [Figure 3](#) shows the speciation as a function of concentration. The Raman analysis of associated TFSI⁻ populations is consistent with the trends: the fraction of CIPs generally decreases and the fractions of free ions increase with increasing concentration, qualitatively similar to the Mg(TFSI)₂ in G2 system. The high-concentration (0.57 M) population experimental data are within 5% of the computed values, but the lower concentrations do not show such agreement. The disagreement suggests that either the computed K_A is overestimated at the lower concentrations or higher-order aggregates could be present (e.g., SSIPs, triple ions), which is discussed further below. The Raman data points indicate a slight increase in ion pairing by 0.6% in going from 0.035 to 0.05 M. However, the error estimate for Raman inferred populations due to instrument noise is 6% at the lowest concentration (0.02 M) and otherwise generally decreases with increasing concentration (error bars are not displayed here for visual clarity; see the [Supporting Information](#)). Thus, here the emphasis is placed on the general trend of decreasing ion pairing with increasing concentration.

At high concentrations, the permittivity of G2 electrolytes is higher than that of G1, despite a similar fraction of ion pairing according to Raman spectroscopy, and this highlights an important difference in CIP structure tendencies. As shown in [Table 1](#), CIPs in G2 show a much larger dielectric increment increase than those in G1 (147 M⁻¹ versus 72 M⁻¹), which allows the electrolyte to reach a higher static permittivity despite having a similar fraction of CIPs. The larger dielectric increment is due to a preference for the more polar monodentate configuration of the CIP in G2, in contrast to the bidentate majority configuration of the CIP in G1 (see the inset illustrations in [Figure 3](#)). In the model used herein, we approximate the majority dentation as the only ion-pair structure, although likely some admixture of both dentations is present in both liquids. The K_A^0 values for the two studied systems (G2 and G1) are on the order of 10⁸ ([Table 1](#)), while for high-permittivity electrolytes typically K_A^0 is much smaller (e.g., on the order of 10²).²⁸ The concentration-dependent K_A values are dramatically lowered from the permittivity increase, a phenomenon specific to low-permittivity systems.

As part of the presented results, a few possible sources of error should be considered and discussed. First, the assumption of a concentration-independent interionic distance parameter α_{DH} could in principle be improved.³⁵ In this work we derive α_{DH} as the sum of radii^{36,37} of a CIP and an anion, providing a reasonable value for a multivalent Mg²⁺ system.³⁵ Second, assuming that CIPs are the only associated species is certainly an approximation, especially in the low-concentration regime. For previous multivalent systems, SSIPs were shown to be present at low concentrations (below 0.2 M),²⁸ which may explain the disagreement at low concentration for the Mg(TFSI)₂ in G1 and G2 systems. Unfortunately, the low-frequency limit of DRS and the Raman analysis methods (which cannot distinguish between free ions and SSIPs and show higher errors at lower concentrations) preclude us from directly investigating the presence of SSIPs in this work. Moreover, the agreement between the MSM and the DRS and Raman analyses at higher concentrations supports the

assumption of CIPs as the majority associated species at higher concentrations.

Importantly, for both the G1 and G2 electrolyte systems, the calculated values of the permittivity and speciation and the respective experimental data are consistent with the redissociation hypothesis. More precisely, the permittivity increase, in addition to the increasing ionic strength, which enhances screening of free ions and lowers their chemical potential (via [eq 4](#)), explain the dramatic stabilization of free ions at higher concentrations.

In contrast to high-permittivity Li ion electrolytes, multivalent electrolytes for battery applications, which generally use low-permittivity solvents, show an increasing molar conductivity with increasing concentration. To improve our understanding of the complex speciation in these liquids, we have used modeling and DRS to establish an increase in static permittivity as a function of salt concentration in Mg(TFSI)₂/G1 and G2 electrolytes. Furthermore, the speciation diagrams constructed from the multiscale modeling methodology show an increase in the fraction of dissociated species with concentration, which is confirmed experimentally by Raman spectroscopy. The combined evidence strongly indicates that polar contact ion pairs that form at low concentration trigger a redissociation mechanism, leading to an increase in free charge-carrier ions at higher concentrations. For G1, the dramatic change in speciation from redissociation may also play a role in the miscibility gap from 0.05 to 0.57 M.¹⁵ Furthermore, the current results suggest that for low-permittivity multivalent electrolytes, redissociation is a non-specific effect (i.e., independent of the salt chemistry), provided that a considerable population of strongly polar associated species persists. Preliminary measurements indicate that many Mg²⁺ and Ca²⁺ electrolytes of interest exhibit increasing molar conductivity with concentration, and further investigations linking these observations to the attendant cluster structures and populations will be the subject of future publications. Finally, the ability to tune redissociation—and therefore speciation and transport—via designer salt additives remains a viable path forward.

METHODS

Infinite-dilution association constants K_A^0 , shown in [Table 1](#), were calculated via first-principles quantum-chemistry calculations. Hybrid DFT calculations were undertaken with Gaussian 016 software³⁸ using the ω b97x-d functional³⁹ with the def2tzvp basis set⁴⁰ and a continuum solvation model⁴¹ (CSM) using the neat solvent permittivity as well as an explicit first solvation shell for cations. Before geometry optimization via ab initio methods, initial configurations were picked via conformational analysis using MacroModel⁴² and an OPLS-based force field,⁴³ where structures with dentation matching those from the classical MD simulations were picked. In order to correct for spurious contributions of low-frequency modes to the vibrational partition function, Truhlar's correction⁴⁴ was applied using Patton's code.⁴⁵ $f_{e,A}$ was calculated using the optimized geometries of the neat solvent and then single-point calculations as the permittivity of the CSM was varied. A function as described by [eq 5](#) was fit (further details are provided in the [Supporting Information](#)). This yielded an analytic function allowing the computation of the correction to the association constant due to the change in permittivity.

In order to calculate $\Delta\epsilon_i$, MD simulations were undertaken with GROMACS⁴⁶ as described in a previous publication.³³

Briefly, each simulation held a single salt species in a box of solvent such that the concentration was 0.1 M. In order to include the contribution of salt species to the total permittivity via the fluctuation–dissipation theorem, the dipole of the salt species had to be drawn and included in the total polarization. This was undertaken with an in-house code as described and provided in the previous publication.³³ As was necessary, certain of the simulations carried an overall charge, for which the GROMACS software provided a correcting background homogeneous charge.^{46,47} For charged associated salt species, the net charge was subtracted at the center of mass.⁴⁶ Briefly, the dipole moment \mathbf{P} of the associated salt species can be written as follows:

$$P_{\text{salt species},x} = \sum_{\text{ions}} q_{\text{ions}} r_x \quad (7)$$

in which “ions” refers to the atomic point charges of the salt species and x indicates the given Cartesian direction. If the associated salt species has an overall charge, then the contribution from the center of mass (COM) charge can be subtracted:

$$P'_{\text{salt species},j} = P_{\text{salt species},j} - r_{\text{COM}}(\sum_k q_k) \quad (8)$$

Electrolyte solutions for ionic conductivity, DRS, and Raman measurements were prepared in an argon-filled glovebox (MBraun) with $\text{H}_2\text{O} < 1$ ppm and $\text{O}_2 < 0.1$ ppm. The solvents 1,2-dimethoxyethane (G1) and diethylene glycol dimethyl ether (G2) were purchased in anhydrous form from Millipore-Sigma, distilled, and stored over 3 Å molecular sieves with activated alumina. $\text{Mg}(\text{TFSI})_2$ (Solvionic, 99.5%) was dried under vacuum at 170 °C for a minimum of 48 h prior to use. It was found that the dissolved $\text{Mg}(\text{TFSI})_2$ salt imparted a nontrivial solution volume increase over that of the pure solvents, and thus, careful measurement of the overall solution volume was required in order to obtain accurate molarity values. This was particularly important for solutions of moderate to high concentration. Consistent with a previous report, we found that $\text{Mg}(\text{TFSI})_2/\text{G1}$ solutions exhibited a significant miscibility gap between ~ 0.05 M and ~ 0.57 M, precluding measurements at intermediate concentrations.¹⁵

Solution ionic conductivities were measured in the aforementioned glovebox using an AC impedance system incorporating a homemade conductivity probe consisting of two parallel Pt electrodes. The cell constant of this conductivity probe was periodically calibrated in KCl solutions of various concentrations to ensure measurement accuracy.

Raman spectroscopy was performed in sealed vials on a WITec confocal Raman microscope using a 532 nm excitation laser. The TFSI^- speciation was measured through careful spectral fitting of the TFSI^- breathing mode region (~ 740 cm^{-1}) using Gaussian/Lorentzian line shapes, similar to published methods.^{5,48} Selected examples are shown in the Supporting Information.

Dielectric spectra were measured in glass vials using an immersed slim-form coaxial probe (Keysight N1501A) and a vector network analyzer (Keysight P9375A) over the frequency range from 0.5 to 26.5 GHz. Multiple measurements were made to ensure repeatability, and various immersion depths were tested to confirm the absence of associated artifacts. Calibration was maintained and periodically refreshed using an ECal module (Keysight N7555A). A three-point calibration was performed before each DRS series using air, a short circuit, and tetrahydrofuran.⁴⁹ During spectral acquisition, the samples

were briefly exposed to air (< 1 min). However, no subsequent changes were observed in DRS measurements repeated after long-term exposure to air, indicating that the measurement is insensitive to electrolyte air exposure over these time scales. DRS data were fit with two Debye relaxations for G1 electrolytes and one Cole–Cole relaxation and one Debye relaxation for G2 electrolytes^{50–52} (further details are provided in the Supporting Information).

■ ASSOCIATED CONTENT

Supporting Information

The Supporting Information is available free of charge at <https://pubs.acs.org/doi/10.1021/acs.jpcllett.0c00334>.

Further details on DRS and Raman analysis and the MSM (PDF)

■ AUTHOR INFORMATION

Corresponding Author

Kristin A. Persson – Department of Materials Science and Engineering, University of California, Berkeley, California 94720, United States; Energy Technologies Area, Lawrence Berkeley National Laboratory, Berkeley, California 94720, United States; orcid.org/0000-0003-2495-5509; Email: kapersson@lbl.gov

Authors

Julian Self – Department of Materials Science and Engineering, University of California, Berkeley, California 94720, United States; Energy Technologies Area, Lawrence Berkeley National Laboratory, Berkeley, California 94720, United States; orcid.org/0000-0002-5486-9559

Nathan T. Hahn – Material, Physical, and Chemical Sciences Center, Sandia National Laboratories, Albuquerque, New Mexico 87185, United States; orcid.org/0000-0001-6187-4068

Kara D. Fong – Department of Chemical and Biomolecular Engineering, University of California, Berkeley, California 94720, United States; Energy Technologies Area, Lawrence Berkeley National Laboratory, Berkeley, California 94720, United States; orcid.org/0000-0002-0711-097X

Scott A. McClary – Material, Physical, and Chemical Sciences Center, Sandia National Laboratories, Albuquerque, New Mexico 87185, United States; orcid.org/0000-0001-9011-1043

Kevin R. Zavadil – Material, Physical, and Chemical Sciences Center, Sandia National Laboratories, Albuquerque, New Mexico 87185, United States; orcid.org/0000-0002-3791-424X

Complete contact information is available at: <https://pubs.acs.org/doi/10.1021/acs.jpcllett.0c00334>

Notes

The authors declare no competing financial interest.

■ ACKNOWLEDGMENTS

This work was supported by the Joint Center for Energy Storage Research, an Energy Innovation Hub funded by the U.S. Department of Energy. Work at Lawrence Berkeley National Laboratory was supported by the Assistant Secretary for Energy Efficiency and Renewable Energy under Contract DEAC02-05CH11231. We thank the National Energy Research Scientific Computing Center (NERSC) for comput-

ing resources, as well as NIH Grant S10OD023532. Sandia National Laboratories is a multimission laboratory managed and operated by National Technology and Engineering Solutions of Sandia, LLC, a wholly owned subsidiary of Honeywell International, Inc., for the U.S. Department of Energy's National Nuclear Security Administration under Contract DE-NA-0003525.

REFERENCES

- (1) Shterenberg, I.; Salama, M.; Gofer, Y.; Levi, E.; Aurbach, D. The Challenge of Developing Rechargeable Magnesium Batteries. *MRS Bull.* **2014**, *39*, 453–460.
- (2) Attias, R.; Salama, M.; Hirsch, B.; Goffer, Y.; Aurbach, D. Anode-Electrolyte Interfaces in Secondary Magnesium Batteries. *Joule* **2019**, *3*, 27–52.
- (3) Shterenberg, I.; Salama, M.; Yoo, H. D.; Gofer, Y.; Park, J.-B.; Sun, Y.-K.; Aurbach, D. Evaluation of $(\text{CF}_3\text{SO}_2)_2\text{N}$ (TFSI) Based Electrolyte Solutions for Mg Batteries. *J. Electrochem. Soc.* **2015**, *162*, A7118–A7128.
- (4) Ha, S.-Y.; Lee, Y.-W.; Woo, S. W.; Koo, B.; Kim, J.-S.; Cho, J.; Lee, K. T.; Choi, N.-S. Magnesium(II) Bis(trifluoromethane sulfonyl) Imide-Based Electrolytes with Wide Electrochemical Windows for Rechargeable Magnesium Batteries. *ACS Appl. Mater. Interfaces* **2014**, *6*, 4063–4073.
- (5) Giffin, G. A.; Moretti, A.; Jeong, S.; Passerini, S. Complex Nature of Ionic Coordination in Magnesium Ionic Liquid-Based Electrolytes: Solvates with Mobile Mg^{2+} Cations. *J. Phys. Chem. C* **2014**, *118*, 9966–9973.
- (6) Lapidus, S. H.; Rajput, N. N.; Qu, X.; Chapman, K. W.; Persson, K. A.; Chupas, P. J. Solvation Structure and Energetics of Electrolytes for Multivalent Energy Storage. *Phys. Chem. Chem. Phys.* **2014**, *16*, 21941–21945.
- (7) Rajput, N. N.; Seguin, T. J.; Wood, B. M.; Qu, X.; Persson, K. A. Elucidating Solvation Structures for Rational Design of Multivalent Electrolytes—A Review. In *Modeling Electrochemical Energy Storage at the Atomic Scale*; Springer, 2018; pp 79–124.
- (8) Yamada, Y.; Yamada, A. Review—Superconcentrated Electrolytes for Lithium Batteries. *J. Electrochem. Soc.* **2015**, *162*, A2406–A2423.
- (9) Aurbach, D.; Pollak, E.; Elazari, R.; Salitra, G.; Kelley, C. S.; Affinito, J. On the Surface Chemical Aspects of Very High Energy Density, Rechargeable Li–Sulfur Batteries. *J. Electrochem. Soc.* **2009**, *156*, A694.
- (10) Burke, C. M.; Pande, V.; Khetan, A.; Viswanathan, V.; McCloskey, B. D. Enhancing electrochemical intermediate solvation through electrolyte anion selection to increase nonaqueous Li–O₂ battery capacity. *Proc. Natl. Acad. Sci. U. S. A.* **2015**, *112*, 9293–9298.
- (11) Rosenman, A.; Markevich, E.; Salitra, G.; Aurbach, D.; Garsuch, A.; Chesneau, F. F. Review on Li–Sulfur Battery Systems: an Integral Perspective. *Adv. Energy Mater.* **2015**, *5*, 1500212.
- (12) Kubisiak, P.; Eilmes, A. Solvation of Mg^{2+} Ions in $\text{Mg}(\text{TFSI})_2$ –Dimethoxyethane Electrolytes—A View from Molecular Dynamics Simulations. *J. Phys. Chem. C* **2018**, *122*, 12615–12622.
- (13) Kimura, T.; Fujii, K.; Sato, Y.; Morita, M.; Yoshimoto, N. Solvation of Magnesium Ion in Triglyme-Based Electrolyte Solutions. *J. Phys. Chem. C* **2015**, *119*, 18911–18917.
- (14) Baskin, A.; Prendergast, D. Exploration of the Detailed Conditions for Reductive Stability of $\text{Mg}(\text{TFSI})_2$ in Diglyme: Implications for Multivalent Electrolytes. *J. Phys. Chem. C* **2016**, *120*, 3583–3594.
- (15) Salama, M.; Shterenberg, I.; Gizbar, H.; Eliaz, N. N.; Kosa, M.; Keinan-Adamsky, K.; Afri, M.; Shimon, L. J. W.; Gottlieb, H. E.; Major, D. T.; Gofer, Y.; Aurbach, D. Unique Behavior of Dimethoxyethane (DME)/ $\text{Mg}(\text{N}(\text{SO}_2\text{CF}_3)_2)_2$ Solutions. *J. Phys. Chem. C* **2016**, *120*, 19586–19594.
- (16) Sa, N.; Rajput, N. N.; Wang, H.; Key, B.; Ferrandon, M.; Srinivasan, V.; Persson, K. A.; Burrell, A. K.; Vaughney, J. T. Concentration Dependent Electrochemical Properties and Structural Analysis of a Simple Magnesium Electrolyte: Magnesium Bis-(trifluoromethane sulfonyl)imide in Diglyme. *RSC Adv.* **2016**, *6*, 113663–113670.
- (17) Wright, M. R. *An Introduction to Aqueous Electrolyte Solutions*; Wiley, 2007.
- (18) Barthel, J. M. G.; Krienke, H.; Kunz, W. *Physical Chemistry of Electrolyte Solutions: Modern Aspects*; Topics in Physical Chemistry, Vol. 5; Springer, 1998.
- (19) Delsignore, M.; Farber, H.; Petrucci, S. Ionic conductivity and Microwave Dielectric Relaxation of Lithium Hexafluoroarsenate (LiAsF_6) and Lithium Perchlorate (LiClO_4) in Dimethyl Carbonate. *J. Phys. Chem.* **1985**, *89*, 4968–4973.
- (20) Doucey, L.; Revault, M.; Lautié, A.; Chaussé, A.; Messina, R. A study of the Li/Li⁺ couple in DMC and PC solvents: Part 1: Characterization of $\text{LiAsF}_6/\text{DMC}$ and LiAsF_6/PC solutions. *Electrochim. Acta* **1999**, *44*, 2371–2377.
- (21) Borodin, O.; Douglas, R.; Smith, G.; Eyring, E. M.; Petrucci, S. Microwave Dielectric Relaxation, Electrical Conductance, and Ultrasonic Relaxation of LiPF_6 in Poly(ethylene oxide) Dimethyl Ether-500. *J. Phys. Chem. B* **2002**, *106*, 2140–2145.
- (22) Petrucci, S.; Masiker, M. C.; Eyring, E. M. The Possible Presence of Triple Ions in Electrolyte Solutions of Low Dielectric Permittivity. *J. Solution Chem.* **2008**, *37*, 1031–1035.
- (23) Logan, E. R.; Tonita, E. M.; Gering, K. L.; Ma, L.; Bauer, M. K. G.; Li, J.; Beaulieu, L. Y.; Dahn, J. R. A Study of the Transport Properties of Ethylene Carbonate-Free Li Electrolytes. *J. Electrochem. Soc.* **2018**, *165*, A705–A716.
- (24) Marcus, Y.; Hefter, G. Ion Pairing. *Chem. Rev.* **2006**, *106*, 4585–4621.
- (25) Cavell, E. A. S.; Knight, P. C. Effect of Concentration Changes on Permittivity of Electrolyte Solutions. *Z. Phys. Chem.* **1968**, *57*, 331–334.
- (26) Farber, H.; Petrucci, S. Ultrahigh Frequency and Microwave Relaxation of Lithium Perchlorate in Tetrahydrofuran. *J. Phys. Chem.* **1975**, *79*, 1221–1227.
- (27) Farber, H.; Petrucci, S. Electrical Conductance, Ultrasonic Relaxation, and Microwave Dielectric Relaxation of Sodium Perchlorate in Tetrahydrofuran. *J. Phys. Chem.* **1976**, *80*, 327–335.
- (28) Eberspächer, P.; Wismeth, E.; Buchner, R.; Barthel, J. Ion Association of Alkaline and Alkaline-earth Metal Perchlorates in Acetonitrile. *J. Mol. Liq.* **2006**, *129*, 3–12.
- (29) Hwang, S.; Kim, D.-H.; Shin, J. H.; Jang, J. E.; Ahn, K. H.; Lee, C.; Lee, H. Ionic Conduction and Solution Structure in LiPF_6 and LiBF_4 Propylene Carbonate Electrolytes. *J. Phys. Chem. C* **2018**, *122*, 19438–19446.
- (30) Newman, J.; Thomas-Alyea, K. E. *Electrochemical Systems*; Wiley, 2012.
- (31) Shilov, I. Y.; Lyashchenko, A. K. The Role of Concentration Dependent Static Permittivity of Electrolyte Solutions in the Debye–Hückel Theory. *J. Phys. Chem. B* **2015**, *119*, 10087–10095.
- (32) Schlumberger, S.; Bazant, M. Z. Simple Theory of Ionic Activity in Concentrated Electrolytes. *arXiv [Physics.Chemical Physics]*, September 10, 2017, 1709.03106, ver. 1. <https://arxiv.org/abs/1709.03106> (accessed 2020-01-31).
- (33) Self, J.; Wood, B. M.; Rajput, N. N.; Persson, K. A. The Interplay between Salt Association and the Dielectric Properties of Low Permittivity Electrolytes: The Case of LiPF_6 and LiAsF_6 in Dimethyl Carbonate. *J. Phys. Chem. C* **2018**, *122*, 1990–1994.
- (34) Buchner, R.; Hefter, G. T.; May, P. M. Dielectric Relaxation of Aqueous NaCl Solutions. *J. Phys. Chem. A* **1999**, *103*, 1–9.
- (35) Lee, W. H.; Wheaton, R. J. Analysis of Conductance Data for Associated Unsymmetrical Electrolytes. *J. Phys. Chem.* **1978**, *82*, 605–608.
- (36) Marcus, Y. Ionic Radii in Aqueous Solutions. *Chem. Rev.* **1988**, *88*, 1475–1498.
- (37) Salomon, M. Conductance of Solutions of Lithium Bis-(trifluoromethanesulfone)imide in Water, Propylene Carbonate, Acetonitrile and Methyl Formate at 25 °C. *J. Solution Chem.* **1993**, *22*, 715–725.

(38) Frisch, M. J.; et al. *Gaussian 16*, rev. B.01; Gaussian, Inc.: Wallingford, CT, 2016.

(39) Chai, J.-D.; Head-Gordon, M. Long-range Corrected Hybrid Density Functionals with Damped Atom-Atom Dispersion Corrections. *Phys. Chem. Chem. Phys.* **2008**, *10*, 6615.

(40) Weigend, F.; Ahlrichs, R. Balanced Basis Sets of Split Valence, Triple Zeta Valence and Quadruple Zeta Valence Quality for H to Rn: Design and Assessment of Accuracy. *Phys. Chem. Chem. Phys.* **2005**, *7*, 3297.

(41) Tomasi, J.; Mennucci, B.; Cammi, R. Quantum Mechanical Continuum Solvation Models. *Chem. Rev.* **2005**, *105*, 2999–3094.

(42) *MacroModel*; Schrödinger, LLC, 2018.

(43) Jorgensen, W. L.; Maxwell, D. S.; Tirado-Rives, J. Development and Testing of the OPLS All-Atom Force Field on Conformational Energetics and Properties of Organic Liquids. *J. Am. Chem. Soc.* **1996**, *118*, 11225–11236.

(44) Ribeiro, R. F.; Marenich, A. V.; Cramer, C. J.; Truhlar, D. G. Use of Solution-Phase Vibrational Frequencies in Continuum Models for the Free Energy of Solvation. *J. Phys. Chem. B* **2011**, *115*, 14556–14562.

(45) Rodríguez-Guerra, J.; Chen, J. *GoodVibes*, ver. 2.0.2, 2018. DOI: [10.5281/zenodo.1247565](https://doi.org/10.5281/zenodo.1247565)

(46) Abraham, M. J.; Murtola, T.; Schulz, R.; Páll, S.; Smith, J. C.; Hess, B.; Lindahl, E. GROMACS: High Performance Molecular Simulations Through Multi-Level Parallelism from Laptops to Supercomputers. *SoftwareX* **2015**, *1–2*, 19–25.

(47) Hub, J. S.; de Groot, B. L.; Grubmüller, H.; Groenhof, G. Quantifying Artifacts in Ewald Simulations of Inhomogeneous Systems with a Net Charge. *J. Chem. Theory Comput.* **2014**, *10*, 381–390.

(48) Watkins, T.; Buttry, D. A. Determination of Mg²⁺ Speciation in a TFSI⁻-Based Ionic Liquid With and Without Chelating Ethers Using Raman Spectroscopy. *J. Phys. Chem. B* **2015**, *119*, 7003–7014.

(49) Badiali, J.-P.; Cachet, H.; Cyrot, A.; Lestrade, J.-C. Dielectric Properties of Electrolyte Solutions. Lithium Perchlorate Solutions in Tetrahydrofuran + Benzene Mixtures. *J. Chem. Soc., Faraday Trans. 2* **1973**, *69*, 1339.

(50) Cole, K. S.; Cole, R. H. Dispersion and Absorption in Dielectrics I. Alternating Current Characteristics. *J. Chem. Phys.* **1941**, *9*, 341–351.

(51) *Broadband Dielectric Spectroscopy*; Kremer, F., Schönhals, A., Eds.; Springer: Berlin, 2003.

(52) Grosse, C. A. Program for the Fitting of Debye, Cole-Cole, Cole-Davidson, and Havriliak-Negami Dispersions to Dielectric Data. *J. Colloid Interface Sci.* **2014**, *419*, 102–106.